Chemical Science

ROYAL SOCIETY OF CHEMISTRY

PERSPECTIVE

View Article Online
View Journal

Cite this: DOI: 10.1039/d6sc00812g

All publication charges for this article have been paid for by the Royal Society of Chemistry

Received 29th January 2026
Accepted 6th March 2026

DOI: 10.1039/d6sc00812g

rsc.li/chemical-science

Why and when does lattice oxygen participate in oxygen evolution?

Arun Karmakar, *[ab] Asha K. Satheesan [ab] and Subrata Kundu *[ab]

Why does lattice oxygen contribute to the oxygen evolution reaction (OER) in some oxides and hydroxides, while remaining completely inactive in others that seem to have similar electronic properties? This Perspective argues that lattice oxygen redox does not occur merely due to high metal valence or strong metal–oxygen covalency. It only takes place when two linked conditions are met: (i) the oxidation of transition metals reaches an electronic saturation point that adds oxidative charge to oxygen ligands, and (ii) the lattice can structurally adapt to oxygen removal and vacancy healing during turnover. We demonstrate that various surface-engineering strategies-such as doping, creating heterostructures, modifying interlayers, and anchoring single atoms-work together by lowering charge-transfer energy, improving TM–O covalency, and making additional metal oxidation less stable. However, only materials with enough lattice flexibility can turn this electronic state into functional lattice oxygen redox. By separating the electronic basis of oxygen hole formation from the structural need for vacancy accommodation, this Perspective offers a chemistry-based framework that clarifies both the development and the scarcity of the lattice oxygen mechanism in OER catalysts.

1. Introduction

Have we ever considered why lattice oxygen takes part in O–O bond formation in some transition-metal oxides and hydroxides but not in others, even when the same metal redox transitions occur? In many systems, *operando* spectroscopy shows similar oxidation of the metal center, often reaching high valence states during OER conditions. However, one material may produce oxygen through typical adsorbate intermediates, while another activates lattice oxygen and follows the lattice oxygen mechanism (Scheme 1). These observations suggest that just looking at metal oxidation is not enough to explain lattice oxygen participation. The main question is: what electronic and lattice-level factors decide whether metal oxidation stays focused on the metal or shifts to oxygen-centered redox, which leads to the involvement of lattice oxygen?

Oxygen evolution catalysis has traditionally been understood through adsorbate-centered reaction models. In these models, improvements in activity come from adjusting metal–oxygen binding energies in the adsorbate evolution mechanism (AEM) according to the Sabatier Principle.[1–6] However, increasing experimental and theoretical evidence shows that in some oxides and hydroxides, lattice oxygen can directly take part in O–O bonds. This oxygen activation induced reaction pathway is designated as the lattice oxygen mechanism (LOM).[7–10] The LOM offers an entirely different reaction pathway that can avoid the scaling barrier present in the AEM.[11–14] This perspective argues that activating lattice oxygen is not just an incidental property of materials. Instead, it is a predictable result of regulating transition-metal valence within rigid transition metal (TM)-based oxide and hydroxide structures.

By unifying various surface-engineering methods-such as cation and anion doping, interlayer modulation, heterostructure construction, and single-atom incorporation-under one chemistry principle, we showed that all effective pathways to the LOM focus on pushing the active metal center into very high oxidation states. This approach strengthens TM–O covalency and subsequently switches the redox activity from metal-centered to oxygen-centered redox. In this view, modifying the valence state of the active transition metal becomes the key electronic factor that allows access to lattice oxygen redox.

This perspective further clarifies why many catalysts optimized through similar strategies continue to operate *via* AEM: only when metal oxidation exceeds a critical threshold does oxygen hole formation become unavoidable, selectively triggering LOM. Unlike in AEM, where only surface-bound species participate in the formation of an O–O bond without lattice distortion, lattice oxygen oxidation, the creation of oxygen vacancies, and their refilling are an intrinsic part of the LOM mechanism. This difference places dynamic demands on the lattice structure. While AEM places demands only on the adsorption energetics, LOM places demands on the lattice flexibility required for the reversible removal of lattice oxygen without compromising the lattice structure.

[a]Academy of Scientific and Innovative Research (AcSIR), Ghaziabad-201002, India. E-mail: arunkarmakar020@gmail.com; skundu@cecri.res.in; kundu.subrata@gmail.com; Fax: +91-4565241487; Tel: +91-4565241487

[b]Electrochemical Process Engineering (EPE) Division, CSIR-Central Electrochemical Research Institute (CECRI), Karaikudi-630003, Tamil Nadu, India

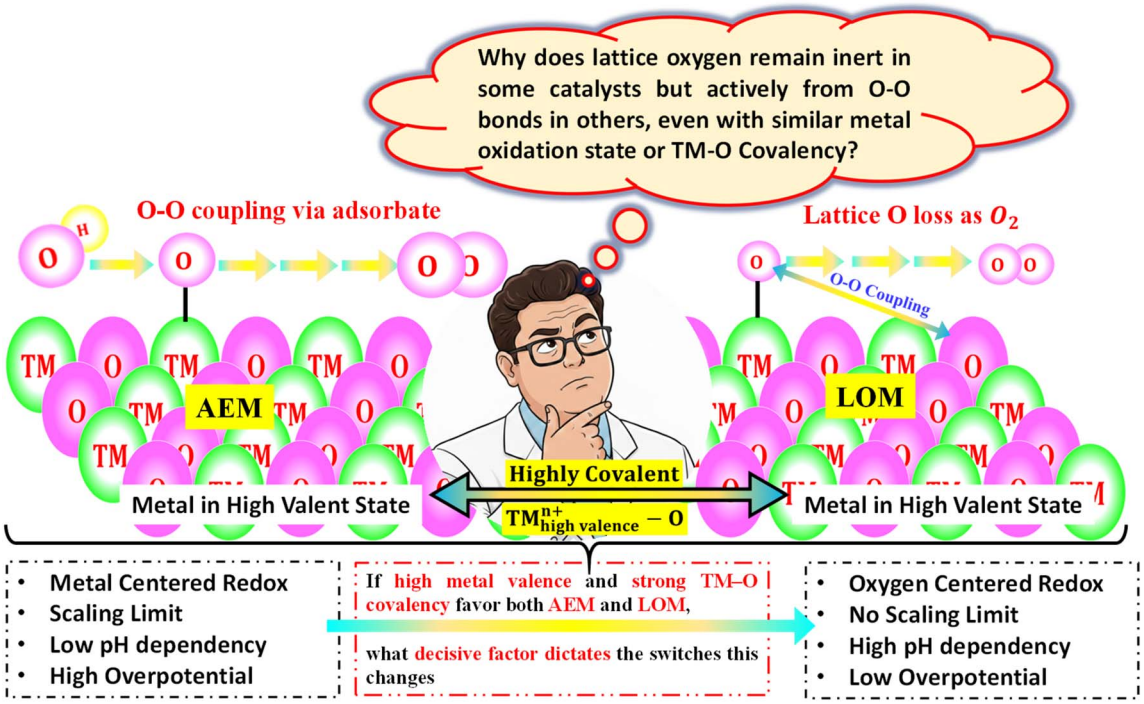

Scheme 1 Conceptual schematic illustrating why comparable metal oxidation states can lead to either AEM or LOM, depending on oxygen redox accessibility and lattice dynamics. Central cartoon created using Google Gemini.

Importantly, electronic activation alone is insufficient; the host lattice must also accommodate oxygen removal and stabilize the resulting vacancies dynamically to sustain lattice oxygen turnover. Using layered double hydroxides (LDHs) as a focal materials platform, this perspective examines how the interplay between metal valence regulation and lattice response governs the emergence and sustainability of lattice oxygen redox. This Perspective emphasizes the identification of the underlying chemical principles that control the occurrence of LOM. By distinguishing the electronic origin of the oxygen hole from the structural need to accommodate a vacancy, we aim to offer a chemistry-based approach that complements, rather than replaces, the experimental diagnostics of LOM, which can rationalize the occurrence of lattice oxygen redox activity. Finding the basic chemical principle that explains when and why lattice oxygen becomes redox-active. Therefore, we do not revisit experimental diagnostics of LOM, such as pH-dependent kinetics, cation effects (for example, KOH *vs.* TMAOH), or isotope-labeling studies, which are now well established. By separating the electronic cause of oxygen hole formation from the structural need for vacancy accommodation, this perspective provides a framework that explains both the incidence and the selectivity of lattice oxygen redox reaction.[15,16]

2. Why are LDHs an ideal platform for this perspective?

LDHs possesses an exclusively adaptable structural and electronic framework that makes them exceptionally well-suited for probing lattice oxygen activation in alkaline OER. Structurally, LDHs consist of positively charged MO_6 octahedral sheets derived from brucite, where divalent (M^{2+}) and trivalent (M^{3+}) metal ions are continuously substituted in a homogeneous solid solution.[17–22] This uniform octahedral coordination-identical for every metal center-stands in sharp contrast to the heterogeneous coordination environments found in spinels (tetrahedral and octahedral sites) or perovskites (A and B-site asymmetry).

In those rigid 3D lattices, the presence of multiple crystallographically inequivalent sites inherently restricts compositional substitution, defect creation, and structural reorganization around active centers. LDHs, by comparison, exhibit a perfectly symmetric coordination environment around all metal ions, enabling far greater flexibility for cation substitution, defect engineering, interlayer modification, and dynamic structural rearrangement during catalysis (Fig. 1). Single-layer or few-layer LDHs exhibit hydroxide conductivities nearly two orders of magnitude higher than their bulk counterparts, and surface modification through exfoliation or nanostructuring further enhances ion and charge transport.[23–25] These features collectively lend LDHs measurably better charge-transfer kinetics than their oxide analogues (*e.g.*, $NiFe_2O_4$, $CoFe_2O_4$), as reflected in consistently lower overpotentials and improved Tafel behaviour.

Chemically, LDHs possess an unusually flexible lattice capable of fine-tuning catalytic function. The coexistence of M^{2+} and M^{3+} ions creates a cooperative redox environment: M^{2+} centers with higher d-band energies preferentially adsorb OH*, while neighboring M^{3+} centers stabilize the higher-valent states formed during anodic polarization. Foreign

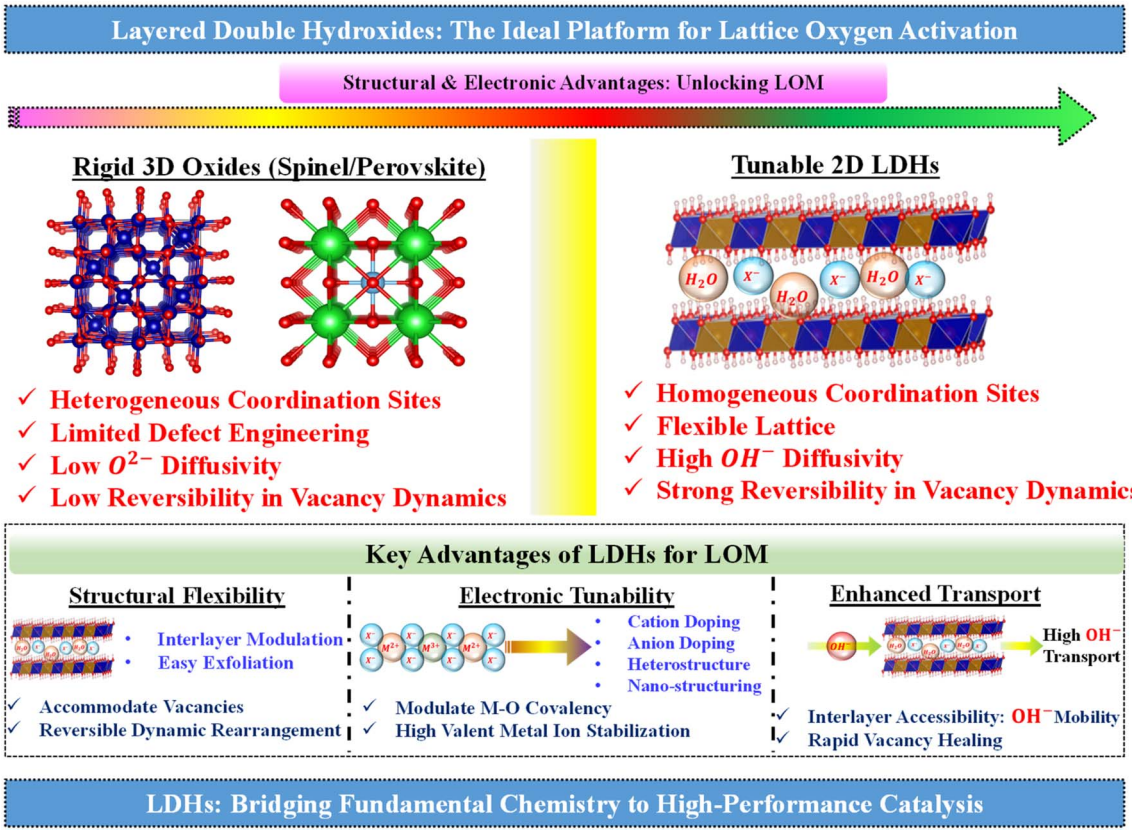

Fig. 1 The figure compares rigid three-dimensional oxides, like spinels and perovskites, with tunable two-dimensional layered double hydroxides (LDHs). In the rigid oxides, mixed coordination environments, limited defect tolerance, and slow oxygen transport favor certain adsorbate evolution pathways. In contrast, LDHs support lattice oxygen mechanisms (LOM) due to their uniform octahedral coordination, structural flexibility, and hydrated interlayers. These characteristics allow for reversible oxygen vacancy formation, quick OH^- transport, and effective lattice oxygen regeneration. The ability to adjust electronic properties through cation/anion doping and defect engineering adds to these benefits. Together, these features enable sustained lattice oxygen redox. Thus, LDHs connect fundamental electronic activation with practical structural flexibility. They serve as an ideal platform for advancing electrocatalysis that involves lattice oxygen.

cation doping-whether redox-active (Fe^{2+}, Mn^{2+}, Co^{2+}) or high-valence (Zr^{4+}, Mo^{6+})-modulates M–O covalency, shifts the d-band center, and tunes oxygen vacancy energetics.[26–30] Interlayer anions further control layer spacing and hydroxide-ion mobility.[31] These structural and chemical freedoms converge to endow LDHs with an electronic softness that is fundamentally distinct from spinels or perovskites. Taken together, the combination of uniform octahedral coordination, structural softness, high hydroxide mobility, cooperative electronic structure, and exceptional defect tunability renders LDHs an incomparable platform for lattice oxygen activation.[32] Their modularity enables decoupling of structural, electronic, and defect-related influences on OER kinetics. This makes LDHs not only mechanistically revealing but also technologically promising as catalysts capable of overcoming the intrinsic overpotential limitations of traditional oxide materials.

Beyond serving as model systems for probing lattice oxygen chemistry, LDHs have emerged as some of the most practically relevant OER catalysts for alkaline and anion-exchange-membrane water electrolysis. Recent studies show that various NiFe-LDHs and their derivatives can sustain industrially relevant current densities at relatively low overpotentials with excellent long-term stability. In several cases matching or surpassing noble-metal benchmarks such as RuO_2 and IrO_2. Therefore, rational access of lattice oxygen activation and stabilization offers an alternative pathway to lower activation barrier for OER beyond what is achievable through adsorbate optimization alone. Thus, LDHs are not only a convenient platform for studying LOM, but a technologically meaningful one in which fundamental control over oxygen redox can translate directly into improved electrolyzer performance (Table 1).

3. Why is the LOM becoming essential beyond traditional AEM pathways?

The traditional AEM has long served as the foundational model for understanding the OER, describing a four-step sequence of proton-electron transfer events *via* surface-bound M–OH*, M–O*, and M–OOH* intermediates. Within this framework, the energetics of OER are tightly governed by the linear scaling relationship between the adsorption energies of OH* and OOH*, which fixes $(\Delta G^*_{OOH} - \Delta G^*_{OH})$ at approximately 3.2 ± 0.2 eV (Fig. 2).[52,53] This locking a theoretical energy barrier of

Table 1 Representative examples of LDH-based catalysts operating in AEM-relevant regimes

S. No.	Catalysts	Overpotential (mV)@j (mA cm^{-2})	Tafel slope mV dec^{-1}	Current density (mA) @ volt	Stability (h)@j (mA cm^{-2})	Reference
1	CAPist-L1	220 ± 4.5; 1000	29.2 ± 2.6	7350; 2	15 200	33
2	RT-NiFe LDH	1460; 500	42.12 ± 2.19	1000: 1.69 V	15	34
3	VCr, Co–NiFeOOH	198; 10 239; 100	39.5	1000; 1–68 V	500@500	35
4	PF_6^--NiFe LDH	209; 200	28.7		5000@1000	36
5	NiFeLDH-[PO_4^{3-}]	—	—	500: 2 V	1000@1000	37
6	NiFe-LDH-PTA	342 ± 9; 1000	83.28	1000@1.93 V	500@1000	38
7	CrO_4^{2-}-NiFeLDH/Cr_2O_3/NF	410; 100	37.2	100@1.56 V	2500@1000	39
8	NiMoN/NiFeLDH	266; 1000	42.2	1000@2.29 V	250@1000	40
9	RuMoNi	245; 10	41.2	1000@1.72V	3000@500	41
10	Ru–S NiFe LDH	279; 100	81.65	1500@2V	80@1000	42
11	NFA-CA	169; 10	49	2000@1.79 V	1000@1000	43
12	NiFeMo-LTH/MXene	340; 100	56	750@2.16 V	60@100	44
13	Co, Mo–NiFe LDH	255; 100	43	2000@1.94	130@2000	45
14	z-NiFe	190; 1000	28.5	1000@1.76 V	14 000@1000	46
15	$Co_{2.8}$, $W_{3.8}$-NiFeLDH	255; 1000	37.8	1000@1.86 V	300@1000	47
16	NiFe-LDH/Ni_4Mo	192.5; 10	42	100@1.68 V	150@100	48
17	NiFePx	234; 10	41.2	300@2.15 V	100@300	49
18	NiCrFeMo LDHs	236; 10	91.2	1000@1.87 V	100@500	50
19	ePt/NiFe LDH	325; 500	37	100@1.54 V	1440@500	51

about 1.6 eV (which corresponds to minimum overpotential value of 370 mV) for both M–OH* deprotonation and M–OOH* formation *via* O–O coupling. Numerous strategies such as multi-metallic interfaces, heterostructures, electronic modulation, and defect engineering-have attempted to break this scaling constraint, yet even with such advances, materials following purely AEM-based pathways remain bound by the same energetic bottleneck.

However, several experimental evidence challenges the sufficiency of AEM as a universal descriptor. Highly active catalysts frequently exhibit OER behavior that violates AEM predictions-showing overpotentials below the theoretical limit, pronounced pH dependencies, and non-concerted proton–electron transfer characteristics.[54] Structural and electronic tuning of bulk oxides, such as raising the O 2p-band center or enhancing M–O covalency, have been shown to dramatically accelerate OER kinetics without directly modifying surface adsorption energies, suggesting that bulk electronic structure-not just surface binding-plays a decisive role. Even more compelling are isotope-labelling and *operando* mass spectrometry studies on materials such as $NiCo_2O_4$, IrO_2, RuO_2, and CoPi, which reveal that evolved O_2 can originate not only from

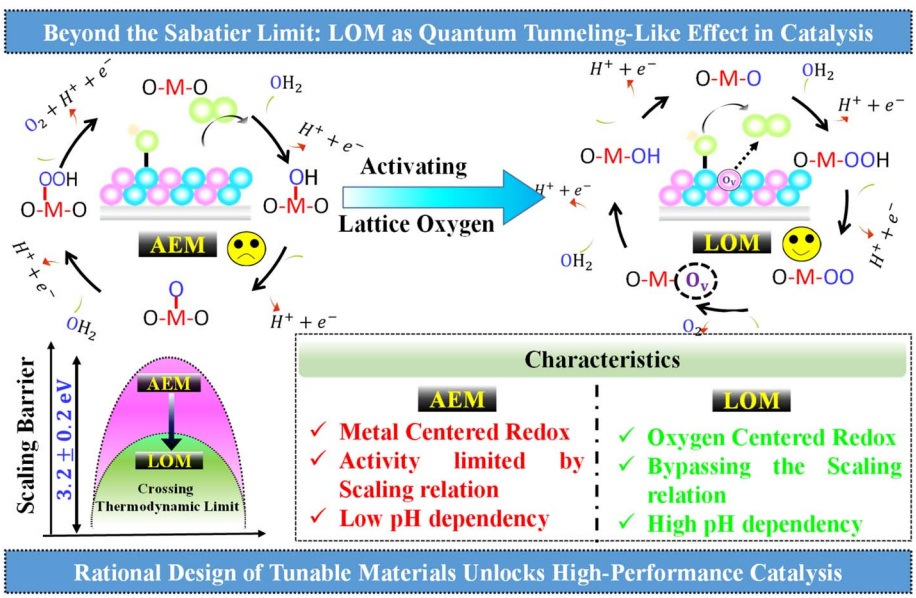

Fig. 2 The schematic compares the adsorbate evolution mechanism (AEM), which is limited by metal-centered redox and the strong *OH/*OOH scaling relationship (about 370 mV overpotential), with the lattice oxygen mechanism (LOM). The LOM serves as a shortcut similar to quantum tunneling by switching to oxygen-centered redox.

water molecules but also from oxygen atoms intrinsic to the lattice.[54–59] These observations collectively challenges the core AEM assumption of a static, spectator oxide lattice and instead point toward the active participation of lattice oxygen in the reaction. This example shift has led to the emergence of the LOM, wherein strongly hybridized M–O bonds and oxidizable oxygen ligands facilitate the formation of lattice oxygen holes ($O^{-}/O^{\bullet -}$), transient oxygen vacancies, and peroxo-like O–O species directly within the lattice network.

Yet, despite its transformative potential, LOM remains difficult to control and predict. Activation of lattice oxygen typically requires highly oxidizing potentials, rendering the process thermodynamically demanding and, in many cases, structurally destabilizing. Consequently, rational LOM engineering demands materials platforms that permit fine control over metal–oxygen covalency, enable reversible oxygen vacancy formation, and provide sufficient lattice flexibility to accommodate oxygen redox without irreversible degradation. Developing catalysts that can stably sustain high metal oxidation states while allowing dynamic and reversible lattice oxygen participation therefore remains one of the most pressing challenges in contemporary OER research. Addressing this challenge will require a shift from empirical activity optimization toward deliberate electronic- and lattice-level design principles that couple redox chemistry with structural resilience.

4. What electronic factors enable the lattice oxygen mechanism?

During OER, in the AEM pathway, water (acidic condition) or hydroxide ions (alkaline condition) adsorbs over active metal center and subsequent losses of protons takes place step by step. This process forms HO*, O*, and HOO* intermediates before releasing O_2. However, this pathway assumes that the oxygen lattice is passive and does not change during catalysis. In the LOM pathway, OER cycles proceeds through the adsorption of OH^{-}/H_2O into oxygen vacancies. Then, lattice O^{2-} reacts with the adsorbed oxide species to form O–O bonds, and subsequently the oxygen species from the electrolyte occupy the vacancy site. This redox cycling of lattice oxygen, closely linked to surface changes and vacancy dynamics, is the key feature of LOM catalysis in both acidic and alkaline environments.

4.1. Electronic preconditions for activating lattice oxygen

The activation of LOM on an electrocatalyst requires an electronically accessible and redox active oxide ligand coordinated with the metal centers. Recent *operando* spectroscopy and isotope labelling studies show that certain high-performing oxides and (oxy)hydroxides could successfully activate the oxide ligand.[60] This creates lattice oxygen holes $O^{(2-\delta)-}$. The activation oxide ligands requires some electronic prerequisite to be hold in transition metal (TM)-based electrocatalysts:

(a) Highly oxidized TM centers which possesses high electronegativity (χ) and can withdraw electron density from the coordinated oxygen.

(b) Strong TM–O covalency, which permits efficient mixing of TM d orbitals with O 2p orbitals. Effective orbital overlap reduces the energy gap between metal d and O-2p states which facilitate the oxygen-hole formation.

(c) Band structures where O 2p states are close to or above TM d states, enabling oxygen to take part directly in redox processes.

These electronic features contrast with AEM catalysts, where oxygen remains an anion and electron transfer mainly occurs on TM centers.

4.2. Why only certain oxides/hydroxides meet the electronic criteria for LOM

The electronic requirements mentioned earlier, such as high-valent TM, strong TM–O covalency, and position of O 2p band relative to TM d states, are interconnected. These prerequisites are the manifestation of underlying TM–O band structure. These characteristics arise naturally from the electronic arrangement of the octahedral TMO_6 building block which ultimately determines whether oxygen can accumulate holes and undergoes redox reactions.[60] The hybridization between TM d and O 2p orbitals produces bonding (M–O) and antibonding (M–O)* states (Fig. 3). Strong inter-electronic repulsion in the M-O* state lead to formation of low and high energy lower Hubbard band (LHB) and upper Hubbard band (UHB) respectively. Within this outline, two key factors control whether the material meets the electronic criteria for LOM:

(a) Charge-transfer energy ($\Delta = \varepsilon_{\text{TM-nd}} - \varepsilon_{\text{O-2p}}$) which signifying the energy difference TM nd and O 2p band in the bonding state with respect to Fermi level (E_F). A highly positive Δ with very low lying O 2p band signifies an increased ionic character in the TM–O bond. This electronic condition greatly stabilized the O 2p band and thereby electron transfer preferably occurs metal redox center. While a small or negative Δ corresponds to the requirement that O 2p states are close to or above TM d levels with increased covalency, allowing the formation of oxygen hole.

(b) On-site Coulomb repulsion (U) represents the energy cost of adding an electron to the TM's nd orbital. Higher oxidation states increase U through orbital contraction, satisfying the requirement for highly oxidized TM centers that can pull electron density from oxygen.

The early transition metal and low valent oxide/hydroxide possesses high electronegativity difference ($\Delta_\chi = \chi_{\text{TM}} - \chi_{\text{O}}$) with oxide ligand which lead to highly positive Δ value places O 2p band well below the TM nd band. This makes the O^{2-} ligands to be redox inactive. Further with larger ionic TM–O bond the material behaves as a Mott-Hubbard insulator ($U < \Delta$) and make it fundamentally incompatible with the requirements for LOM. In contrast, in the late transition metal and high valent oxide/hydroxide, the decreased Δ_χ induces strong covalency in the TM–O bond. Moreover, increased orbital contraction prompts the inter-electronic repulsion and thereby brings the LHB closer to O 2p band. This overlap of LHB into O 2p band sets the precise electronic condition towards electron transfer from the O to the metal center and thereby promotes the

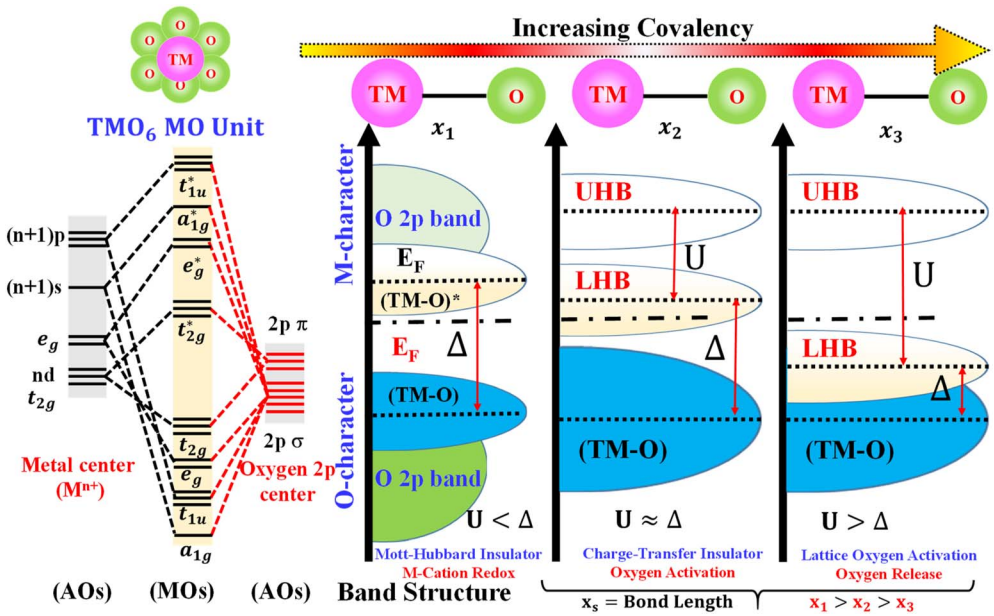

Fig. 3 Schematic illustration of the evolution of the molecular orbital structure of an octahedral TMO_6 unit and the corresponding solid-state band structure as a function of TM–O covalency. Increasing covalency (shorter TM–O bond length) enhances O 2p-TM d hybridization, driving a crossover from metal-centered redox to oxygen-centered redox and enabling lattice oxygen activation.

intramolecular O → TM electron transfer. This enables effective oxygen hole, $O^{(2-\delta)-}$ formation and effectively activate oxygen for O–O bond formation. Overall, increased TM–O covalency emerges as the key electronic prerequisite for enabling LOM in OER. By reducing the charge-transfer energy (Δ) and elevating the O 2p band toward the Fermi level, strong covalency renders lattice oxygen redox-active and kinetically accessible. Consequently, Δ and the energetic alignment of O 2p states serve as quantitative descriptors governing both the onset and efficiency of LOM-driven oxygen evolution. As an illustrative example the computational studies on Co based perovskite and spinels shows that materials favours LOM with negative [($\Delta = \varepsilon_{TM\text{-}nd} - \varepsilon_{O\text{-}2p}$] and higher absolute O 2p band energies. This rigorous electronic balance explains why only select oxides and hydroxides can access the LOM pathway set the stage for material platforms capable of meeting these demands. The above electronic requirements explain why lattice oxygen redox-and consequently LOM-emerges only in limited class of oxide/hydroxide electrocatalysts. The apparent selectivity towards the LOM is not incidental but a consequence of fundamental electronic structure constraints that only certain oxide/hydroxide can satisfy.

5. Why layered double hydroxides provide an ideal electronic landscape for lattice oxygen redox

Having established that the lattice oxygen mechanism in OER demands a subtle convergence of highly oxidized metal centers, strong TM–O covalency, and favorable energetic alignment between O 2p and TM d states, an important question naturally emerges: *why should LDHs offer a more compelling platform for lattice oxygen activation than conventional perovskite or spinel oxides, where LOM has primarily been identified?* Addressing this question requires moving beyond phenomenological observations and toward a chemistry-driven understanding of how lattice oxygen redox can be deliberately enabled and controlled. In this context, LDHs occupy a uniquely advantageous position. By framing lattice oxygen activation through fundamental electronic and chemical descriptors rather than isolated material examples, the discussion that follows reveals how LDHs not only satisfy the established prerequisites for LOM but also offer a chemically programmable platform to rationally design and regulate oxygen-centered redox processes. This chemistry-centric perspective provides a unifying framework for understanding LOM activation across LDHs and outlines clear pathways for advancing next-generation OER electrocatalysts.

5.1. High-valent metal ions induced lattice oxygen activation

Increasing the oxidation state of the active metal centers is one of the most impactful strategies for enabling LOM in the OER. This approach manipulates charge balance within the lattice and paving electronic reorganization and results in increased covalency in the TM–O bond. A more thermodynamically directed route towards high valent TM active site involves doping of a foreign cation with higher redox potential than the host metal ions. The intrinsic redox equilibrium driving the spontaneous electron transfer from the host metal ions to the oxidizing dopant species as follows:

$$TM_{host}^{n+} + D^{m+} \rightleftharpoons TM_{host}^{(n+1)} + D^{(m-1)+}$$

This intrinsic redox coupling stabilizes the high-valent metal ions even under mild synthesis or electrochemical condition. Strong electron withdrawing effect on coordinated oxygen facilitate the oxygen hole formation effectively with lower Δ value and thereby could promote the LOM in OER. As an illustrative example, the doping of highly oxidizing and high valent Mo^{6+} species in CoFe-based layered hydroxide induces an effective LOM in OER.[61] Experimental and theoretical analyses reveals an effective transformation of active Co species to its high valent counterpart by the electron withdrawing and oxidizing effect exerted by Mo species. Similarly in another report Chen and co-workers studied similar high-valent Mo doping induced activation of NiFe-LDH nanosheet towards the LOM in OER.[62] XPS analysis reveals the presence of high content Ni^{3+} ions in MoNiFe-LDH structure upon redox reaction induced electron transfer from the Ni^{2+} to Mo site and it is clearly observed from the voltammetry analysis (Fig. 4a and b). Theoretical analysis further supported the LOM pathway where density of state (DOS) analysis shows an O 2p band position of -1.58 and -1.4 eV in pristine and Mo doped structure respectively. The Mott-Hubbard splitting analysis reveals an increase in U value from 6.38 eV to 7.58 eV upon Mo doping (Fig. 4c). Wang and co-workers executed same high-valent Mo doping assisted transformation to high valent Ni and Fe species.[63] Here in this work the authors executed an innovative surface atom release speed mediated doping of Mo ions in bimetallic hydroxide by controlled dissolution of Mo atom from Mo_2N surface that schematically shown in the Fig. 4d. XPS and X-ray adsorption (XAS) analysis confirmed the transformation of Ni and Fe to their high-valence state (Fig. 4e and f). From the OER polarization curve it shows higher activity with lower overpotential and TOF calculation reveals an increase in intrinsic activity by 8.1 times upon Mo doping (Fig. 4g and h). Experimental and theoretical analysis reveals this particular surface modification technique facilitate the LOM pathway and thereby reduces the activation energy towards the OER. The DOS calculation reveals the upshifting of the O 2p band to -1.29 eV from -1.46 eV relative to Fermi level. The d–d coulomb interaction analysis reveals the U value change from 4.91 and 7.78 eV to 5.38 and 8.09 eV for Ni and Fe respectively upon Mo doping in the hydroxide structure. Such an enlarged U value of Ni/Fe ensure the downshift of LHB, facilitate the electron flow O to TM and thereby activation of lattice oxygen becomes feasible kinetically (Fig. 4i). Thus redox reaction induced activation of active metal center increases the electronegativity difference with bonded oxygen ($\Delta_\chi\downarrow$) and hence, increases covalency in the TM–O bond. Upwards shifting of O-2p band towards the Fermi level and thereby reduced the Δ value. Additionally increased U successfully promotes the intramolecular O $\rightarrow$ TM electron transfer and reduce the activation energy towards oxygen activation.

5.2. Low-valent metal ions induced lattice oxygen activation

Introducing low-valent cations into TM oxide/hydroxide structure creates a local charge deficiency and for the sake of compensating the increased positive charge density the change in electronic structure of metal ions takes place. If the dopant (D) is electrochemically inactive, the charge compensation would occurs through the oxidation of active TM centers as follows:

$$TM_{host}^{n+} + D^{(n-1)+} \rightarrow TM_{host}^{(n+1)} + e^-$$

The electronic restructuring increases the average oxidation state of host TM ions, leading to contraction corresponding d orbitals with increased overlap with O 2p orbital. As result of strength TM–O bond lowers the Δ and thereby activated the lattice oxygen without destabilizing the lattice. Although this strategy has not yet been systematically explored in LDH-based materials, several illustrative examples from oxide and oxyhydroxide systems underscore its effectiveness. These precedents provide valuable chemical insight and establish a compelling direction for future efforts to engineer lattice oxygen redox activity within LDH frameworks. For instance, Zhou *et al.*, developed low-valent Cu ion doped CoOOH materials for promoting LOM pathway in OER.[64] XAS analysis in Co–K edge spectrum provided a strong evidenced for the transformation of Co^{3+} species to $Co^{3.25+}$ in presence of low Cu ions. In term of electrochemical performance the $Cu_xCo_{1-x}OOH$ delivers a high intrinsic activity than the pristine CoOOH (6.5 times increase in TOF value was observed). Though a direct theoretical correlation for various electronic parameters such as Δ, U and other was not produced, various experimental observation proves the occurrence of lattice oxygen mediated OER in $Cu_xCo_{1-x}OOH$. Electrochemically inert Sr^{2+} ion doping in $LaCoO_3$ perovskite structure induces the oxidation of Co^{3+} ions to Co^{4+} ions and subsequent increase in OER activity was observed through lattice oxygen activation.[65]

5.3. Anion doping activated lattice oxygen

Anion substitution offers a powerful and unique way to manage lattice oxygen activation by directly changing the local electronic environment of the transition metal–oxygen framework. Unlike cation doping, which mainly adjusts the oxidation state of metal centers, anion doping modifies the electron density distribution, polarizability, and covalency of the metal–ligand bond. This change affects how easily oxygen-centered redox occurs. Incorporating low-electronegativity, highly polarizable anions like P^{3-}, S^{2-} into oxide or hydroxide lattices boosts the electron density around nearby transition-metal centers.[66] This electron donation stabilizes lower metal oxidation states and decreases the oxidation potential of the active metal sites. Meanwhile, the high polarizability of S^{2-} expands and raises the energy of the ligand p states. This can indirectly elevate the effective O 2p band of nearby oxygen ligands by improving orbital delocalization. As a result, lattice oxygen becomes more electronically mobile, which lowers the energy needed for hole formation and helps oxygen participate in the oxygen evolution reaction (OER). For instance, Su and co-worker has modified the LOM pathway in NiCr-LDH *via* S^{2-} doping (Fig. 5a).[67] Valence state of active metal centers before and after S^{2-} doping *via* XPS analysis which reveals no substantial shift in Ni 2p XPS maxima

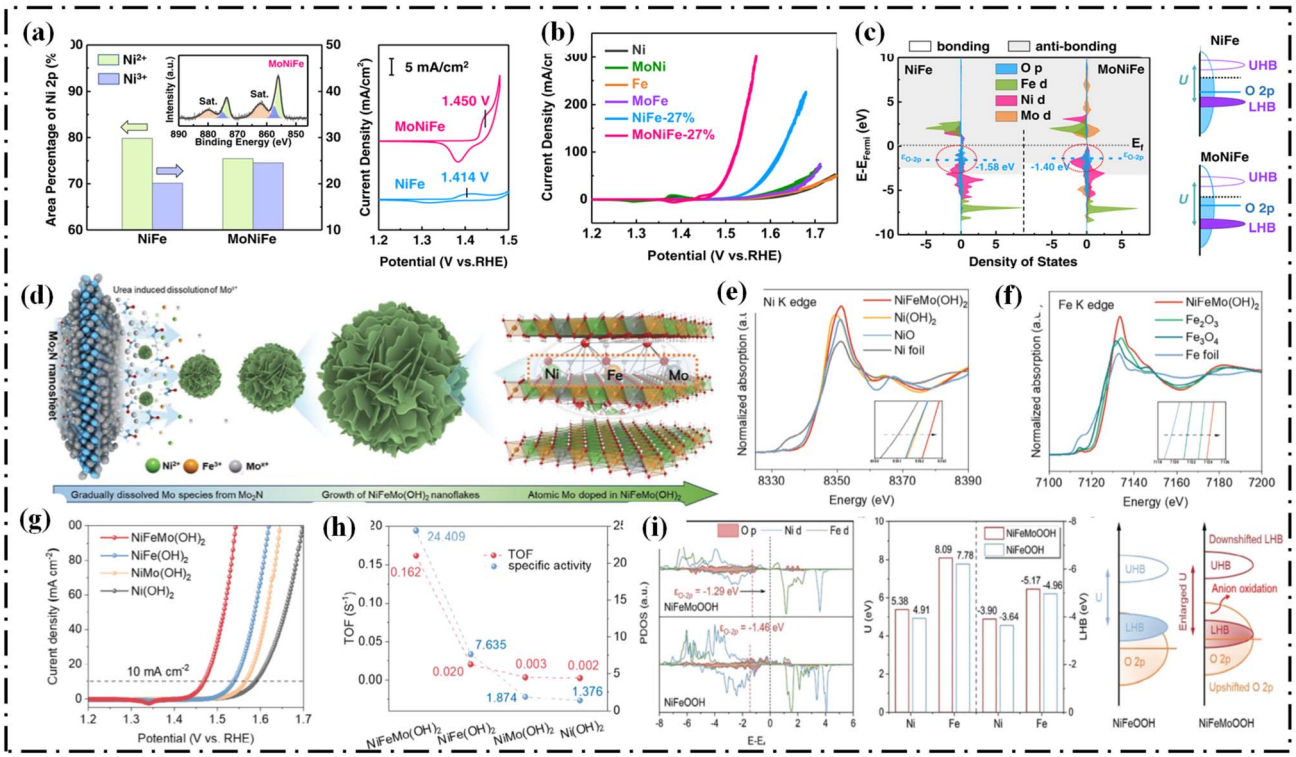

Fig. 4 (a) Ni 2p XPS spectra and corresponding Ni redox peaks from CV of NiFe and MoNiFe (oxy)hydroxides; (b) CV polarization curves; (c) projected density of states (PDOS) and schematic band structures of NiFe and MoNiFe (oxy)hydroxides, highlighting antibonding states below the Fermi level and Hubbard band splitting; reproduced from ref. 62 with permission from [Nature Publisher], copyright [2022].; (d) schematic illustration of the substrate-assisted growth of $NiFeMo(OH)_2$; (e and f) Ni and Fe K-edge XANES spectra; (g and h) OER polarization curves in 1 M KOH, TOF, and specific activity at 300 mV overpotential; and (i) DFT analysis of NiFeMoOOH and NiFeOOH, including PDOS, calculated Hubbard *U* values, LHB center positions, and corresponding band diagrams; Reproduced from ref. 63 with permission from [Wiley], copyright [2025].

with equal proportion of Ni^{3+}/Ni^{2+} ratio. However, upon electrochemical activation (100 cyclic voltammetry cycle), the doped anions further facilitate the Cr ions leaching (cationic vacancy). As a result a profound increase Ni^{3+}/Ni^{2+} ratio was evidenced in the surface reconstructed LDH material. To further verify the role S^{2-} ions, the pristine NiCr-LDH was subjected to same activation and found Ni^{3+}/Ni^{2+} ratio was comparatively lower (Fig. 5b). This indicates, S^{2-} effectively induces the activation of Ni^{2+} to Ni^{3+} ions and satisfying primary electronic condition to favour LOM. The S^{2-} doped reconstructed LDH possesses a lower overpotential value of 244.4 mV overpotential whereas undoped reconstructed LDH demand an overpotential value of 285.4 mV at 100 mA cm^{-2} current density (Fig. 5c). The effect of sulfur doping on the covalency of the Ni–O bond was analyzed by calculating the crystal orbital Hamiltonian pooch (COHP). Larger COHP value of 0.53 for S-doped structure reveals higher covalency in Ni–O bond (Fig. 5d). Strong electron polarizability effect of S^{2-} ions induced a upshifting of O 2p to −2.85 eV from −3.05 eV. These combined electronics benefit successfully promotes LOM pathway in S^{2-} doped reconstructed NiCr-LDH (Fig. 5e). A related anion-driven electronic effect was reported by Li *et al.*, in a bimetallic NiFe-mixed metal oxide (surface reconstructed to oxyhydroxide species during electrochemical reaction) where the activation of the lattice oxygen was promoted *via* P^{3-} ion doping.[68] Although this system does not involve LDHs, it provides a strong chemical comparison to S^{2-}-doped hydroxide lattices. It shows how low-electronegativity anions can change the TM–O electronic structure to support the LOM pathway. Introduction of highly polarizable P^{3-} ions improved the electrochemical OER performance by reducing overpotential value to 237 mV while it was 401 mV for pristine materials. The presence of P^{3-} enhances TM–O covalency and promotes stronger mixing of metal 3d and O 2p states, evidenced by a downshift of the Ni 3d band center from −2.4688 to −2.6918 eV (Fig. 5f). This reduced Δ facilitates oxygen activation and stabilizes oxygen–hole formation under OER conditions.

In contrast to these highly polarizable anions, substituting with high-electronegativity anions like F^- creates a different electronic constraint in oxide/hydroxide structure. The strong electron-withdrawing property of F^- improves TM–ligand covalency by stabilizing higher metal oxidation states and causing the TM d orbitals to contract.[69] This contraction lowers the TM nd band center while having a relatively small direct effect on the O 2p band, effectively reducing the charge-transfer energy (Δ). This band realignment enhances TM–O hybridization and encourages charge transfer from oxygen to metal, allowing oxygen ligands to gain partial hole character under anodic polarization. This could be supported by the experimental finding by Li and co-workers where lattice oxygen was

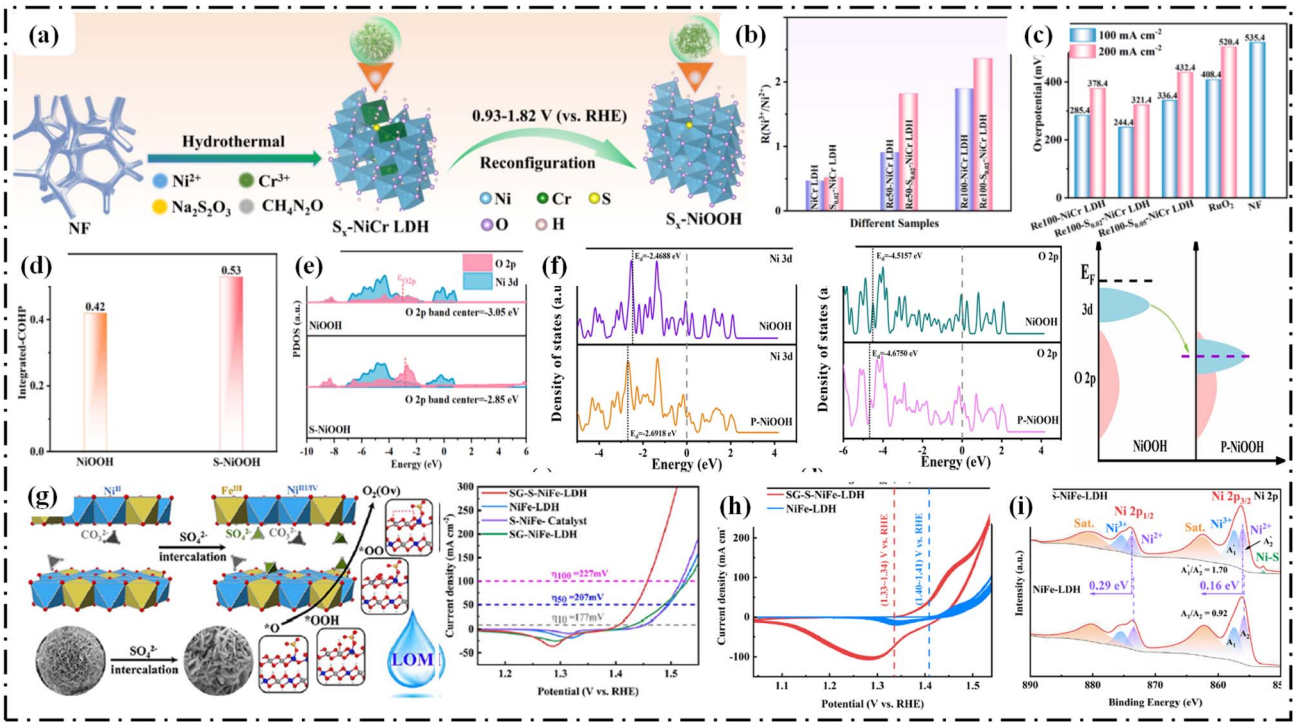

Fig. 5 (a) Schematic illustration of the catalyst synthesis (b) ratio of Ni^{3+}/Ni^{2+}; (c) overpotentials required to reach 100 and 200 mA cm^{-2}; (d) integrated COHP up to the Fermi level for NiOOH and S–NiOOH; (e) calculated projected density of states (PDOS) of NiOOH and S-NiOOH; reproduced from ref. 67 with permission from [Elsevier], copyright [2024]; (f) density of states of Ni 3d and O 2p orbitals, and schematic band structures of P-NiOOH and NiOOH; reproduced from ref. 68 with permission from [American Chemical Society], copyright [2021]; (g) schematic illustration of sulfate-intercalated NiFe-LDH; (h) cyclic voltammetry curves of pristine and sulfate-intercalated NiFe-LDH; and (i) Ni 2p XPS spectra of pristine and sulfate-intercalated NiFe-LDH; reproduced from ref. 72 with permission from [American Chemical Society], copyright [2025].

activated by introducing in F^- ions in the high-entropy FeCoNi-LDH. Synchroton-based XAS analysis was used to monitor the valence state of metal ions before and after the fluoride ion doping. Ni K-edge, Co K-edge, and Fe K-edge spectrum exhibit clear shift towards higher energy upon F- doping, suggesting an increase in the valence state. Fourier transformed extended X-ray absorption fine structure (FT-EXAFS) spectra demonstrate apparent metal–oxygen (TM–O) bond length shrinkages in F-doped LDH compared to pristine LDH, indicating the enhanced covalency. F doping in tri-metallic LDH reduces the overpotential value to 298 mV from 370 mV in pristine LDH. Theoretical analysis reveals that the higher electronegativity of F^- ions induces a downward shift of the Co 3d band center ($\varepsilon_{Co\text{-}3d}$) to −1.349 eV, compared with −1.248 eV in pristine LDH. In contrast to conventional expectations, an exceptional behavior is observed wherein F doping also shifts the O 2p band ($\varepsilon_{O\text{-}2p}$) downward to −3.317 eV from −3.276 eV in the undoped LDH. Despite this concurrent downshift of both bands, the overall reduction in the charge-transfer energy Δ ($\varepsilon_{Co\text{-}3d} - \varepsilon_{O\text{-}2p}$) lowers the energetic barrier for oxygen oxidation, thereby facilitating lattice oxygen activation and promoting the LOM pathway during OER. These two approaches to anion doping-using electron-rich, polarizable anions *versus* strongly electronegative anions-offer complementary methods for activating lattice oxygen. The first method focuses on raising ligand bands and increasing electron delocalization, while the second emphasizes stabilizing metal bands and enhancing covalency. This contrast shows that anion engineering is a flexible and underutilized strategy for adjusting lattice oxygen redox, especially in hydroxide-based systems where anion substitution can occur without causing significant lattice distortion.

5.4. Intercalated-anion modified LDH to activate oxygen redox

From the above discussion it is evident that anion doping in hydroxide lattices has shown potential for lattice oxygen activation in LDHs, similar to what occurs in traditional spinel and perovskite oxides. However unique structural features of LDHs provide an extra and fundamentally different level of flexibility. Having chemically adjustable interlayer space allow the continuous changes without disturbing the metal-hydroxide structure. In contrast to anion doping in dense oxides, interlayer anions in LDHs engage electrostatically and through hydrogen bonding with the brucite-like transition metal–OH sheets. This interaction allows them to indirectly and effectively influence the electronic structure of lattice oxygen and the redox chemistry of the metal centers.

Anions like SO_4^{2-}, NO_3^-, acetate, and PO_4^{3-} can alter the local proton activity, hydrogen-bond network, and charge distribution in the interlayer region. Strongly coordinating or

multivalent anions help to activate the higher oxidation states of transition metals by pulling electron density away from the hydroxide layers. This promotes metal orbital contraction and enhances TM–O covalency. The resulting electronic reorganization lowers the charge-transfer energy (Δ) and aids in localizing holes on oxygen, fulfilling the electronic requirements for lattice oxygen activation.[70,71] This approach is particularly suited for LDHs because interlayer anions can be added or swapped *in situ* using simple electrolytes or precursors. This allows for continuous and reversible adjustments of the electronic structure under operational conditions. The ability to chemically modify the intercalation offers a low-energy method to stabilize high-valent metal states and activate lattice oxygen, all without causing instability in the lattice. This highlights the potential of interlayer anion engineering as a significant yet underused strategy for developing LOM-active LDH electrocatalysts.

For instance Zhang and co-workers reported a sol–gel assisted hydrothermal synthesis of SO_4^{2-} intercalated NiFe-LDH, where intercalates greatly regulate the oxidation state of the active Ni site.[72] The SO_4^{2-} ions promotes the formation of high-valent Ni^{3+} and Ni^{4+} species as evidenced from before and after OER XPS study. Ni^{4+} possesses a closed-shell low-spin d^6 configuration, which facilitate O–O bond coupling. Cyclic voltammetric study reveals the reduction of redox onset potential from 1.33 V *vs.* RHE in presence of SO_4^{2-} ions to 1.40 V *vs.* RHE in pristine LDH (Fig. 5g and h). Therefore, SO_4^{2-} ions promote the transformation Ni^{2+} to high-valent state. The integrated COHP values for Ni sites are −1.08, and −0.99 in presence and absence of the SO_4^{2-} ions respectively. The enhanced covalency in Ni–O bond enables intramolecular charge transfer and thereby activate the lattice oxygen. Qiao *et al.*, executed an interesting study where valence state of Ni and Fe active sites were modulated in SO_4^{2-} intercalated NiFe-LDH to activate lattice oxygen for promoting O–O coupling in OER. XPS studies revealed a positive shift to high binding energy region with 0.2 and 0.8 eV, for Ni and Fe 2p XPS peak respectively (Fig. 5i). These finding verified the increase in Ni and Fe valence state upon SO_4^{2-} intercalation. DOS calculation shows that SO_4^{2-} intercalation induces a marked downward shift of the Fe and Ni d-band centers and thereby reduce the charge transfer energy value and promotes greater covalency in TM–O bond. Moreover, downward shift in LHB from −1.738 eV to −2.291 eV and increased U value induces orbital volume shrinkage. Thus resulting enhancement in TM–O covalency and reduction in Δ render lattice oxygen electronically accessible, thereby promoting OER *via* LOM.

5.5. Hetero-structural engineering for lattice oxygen activation

Heterostructure engineering provides a strong method to activate lattice oxygen redox by electronically coupling different materials that have varying Fermi levels, work functions, and redox properties. In this case, LDHs feature two-dimensional brucite-like sheets and many surface-exposed metal–oxygen sites. This makes them an excellent platform for hosting metallic phases, oxides, chalcogenides, or phosphides. The atomically thin LDH layers increase interfacial contact and ensure short charge-transfer paths, which helps efficient electronic communication across the heterojunction. When a metallic or highly conductive phase is added to an LDH, charge redistributes spontaneously to balance the interfacial chemical potential. This happens because of differences in the electronic structure of the two components. The interfacial electron exchange specifically changes the local electronic environment of the TM–O framework in the LDH, without needing to reconstruct the bulk lattice. As a result, the d-band center of the active metal sites in LDHs can shift away from the Fermi level. This boosts TM–O covalency and lowers the Δ value, creating better electronic conditions for lattice oxygen activation. Cao *et al.*, has carried out a heterostructure engineering on high entropy FeCoNiCrMn-LDH by anchoring CuO oxide nanostructure.[73] Annexation of the CuO nanostructure over high entropy LDH was confirmed from the high resolution transmission electron microscopy (HR-TEM). Mott–Schottky (M–S) analysis reveals the p-type semiconducting nature of CuO structure whereas the LDH structure possesses an n-type electronic behaviour. Therefore upon coupling of two structure the generated build in potential difference allows the electronic transfer from the LDH site to CuO site. Notably, the M–S curve of CuO@FeCoNiCrMn-LDH exhibited both positive and negative slopes, which provides strong evidence for the presence of heterojunction. In terms of OER activity the CuO@FeCoNiCrMn-LDH demands a lower overpotential value of 208 mV compared to pristine CuO and FeCoNiCrMn-LDH at 10 mA cm^{-2} current density value. Stepwise mechanistic investigation from the free energy profile reveals that the herestructure LDH undergoes OER *via* LOM pathway. This was ascribed to the fact that electron transfer from the LDH to CuO site induces a deficiency in electron density over the metal ions and thereby possesses a stronger covalency in the TM–O bond. Which subsequently lowers the Ni 3d band centers to −1.868 eV in CuO@FeCoNiCrMn-LDH from −1.793 eV in FeCoNiCrMn-LDH. Moreover, increased covalency induces an upward shift in O 2p band center of CuO@FeCoNiCrMn-LDH (−3.508 eV) as compared FeCoNiCrMn-LDH (−3.692 eV).

He and group constructed Cr_2O_3 functionalized NiFe-LDH for LOM assisted OER in alkaline condition. Successful operation of LOM in heterostructure reduces the overpotential value to 237 mV from 291 mV in pristine LDH which was required to drive 10 mA cm^{-2} current density (Fig. 6a and b).[74] Valance state result from the XPS analysis reveals an increase high-valent (both Ni and Fe) proportion in the LDH/Cr_2O_3 heterostructure. This indicates a build in potential induced electronic exchange from the LDH site to the Cr_2O_3 site. In contrast to the previous result here both Cr_2O_3 and LDH structure behaves as n type semiconducting nature as evidenced from the M–S plot with positive slope. However, high positive slope with rich donor concentration the LDH structure enable successful electron transfer to the Cr_2O_3 site (additionally supported from the DFT analysis). Therefore, formation of this heterostructure induces high-valent state regulation in the Ni and Fe site and thereby set up LOM prerequisite stage for OER. Thus,

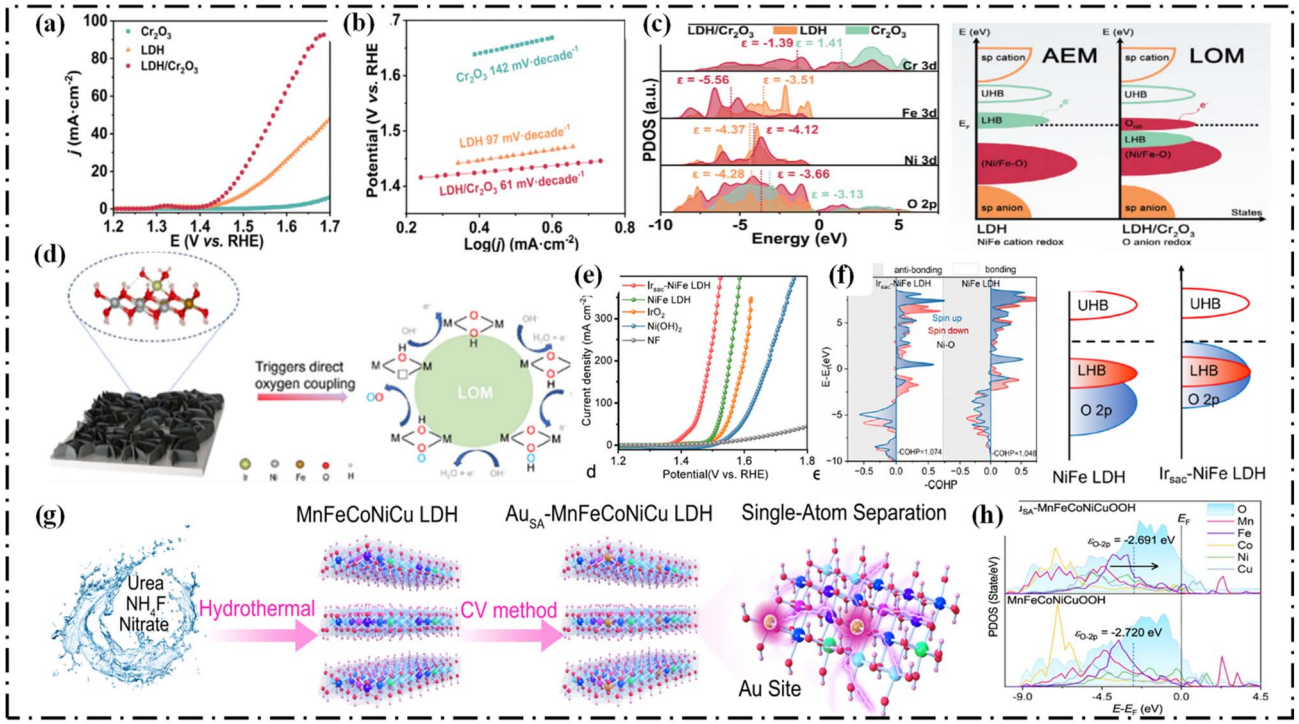

Fig. 6 OER performance in 1 M KOH. (a) LSV polarization curves and (b) corresponding Tafel plots. (c) Projected density of states (PDOS) of Cr 3d, Fe 3d, Ni 3d, and O 2p orbitals for LDH, Cr_2O_3, and LDH/Cr_2O_3, together with schematic energy-band alignment of LDH and LDH/Cr_2O_3 relative to the Fermi level considering Mott–Hubbard splitting; Reproduced from ref. 74 with permission from [Wiley], copyright [2025]; (d) schematic illustration of the synthesis of Ir single-atom-decorated NiFe-LDH (Ir_{SA}-NiFe-LDH). (e) LSV polarization curves in 1 M KOH. (f) Crystal orbital Hamilton population (COHP) analysis of the Ni–O bond in NiFe-LDH and Ir_{SA}-NiFe-LDH, with corresponding schematic band diagrams reproduced from ref. 76 with permission from [American Chemical Society], copyright [2025]; (g) schematic synthesis route of Au single-atom MnFeCoNiCu-LDH (AuSA–MnFeCoNiCu-LDH). (h) Projected density of states highlighting the O 2p band center relative to the Fermi level; reproduced from ref. 77 with permission from [Nature Publisher], copyright [2023].

heterostructure engineering enables controlled redistribution of electron density at active LDH sites through interfacial band alignment. Coupling n-type LDHs with p-type semiconductors or with n-type phases of lower donor density drives electron transfer away from the LDH to equilibrate Fermi levels. This interfacial electron depletion stabilizes higher metal oxidation states, downshifts the TM d-band center, reduces the charge-transfer energy (Δ), and strengthens TM–O covalency (Fig. 6c). Consequently, oxygen ligands become redox-active, favoring lattice oxygen participation over conventional adsorbate-mediated OER pathways.

5.6. Single atom based surface modification

Nanoparticle-based surface nanostructuring of LDHs can modulate local charge distribution near active sites, but its role in promoting LOM during OER remains largely unexplored. In contrast, single-atom-anchored LDHs have been more widely investigated, as isolated metal atoms induce strong localized electronic perturbations that favor lattice oxygen activation.[75] When different SAs are anchored over LDH hosts, the electronic modulation arises from local coordination bonding induces charge redistribution rather than long-range band alignment as in heterostructure. Owing to the unsaturated coordination environment of SAs (usually 4d or 5d TM) and large χ or work function difference with the host metal ions (usually 3d TM), these atoms act as strong electronic perturbators. This results in electron depletion of adjacent TM–O units and thereby activate neighboring oxygen ligand. The SAs stabilizes in high-valent or partially positively charged states, like $Ir^{\delta+}$ and $Au^{\delta+}$. These states pull electron density from surrounding TM–O bonds. This localized electronic compression lowers the TM d-band and/or destabilizes nearby O 2p states and reduces the Δ. For instance, Zhu *et al.*, investigated the effect of Ir SA over the NiFe-LDH structure specifically on the Fe site.[76] Ir_{SA}-NiFe-LDH possesses an ultra-low overpotential value of 213 mV whereas pristine NiFe-LDH demands an overpotential value of 286 mV to drive 50 mA cm^{-2} current density (Fig. 6d and e). Ni and Fe K-edge analysis in XAS reveals that the edge spectrum shifted to the higher energy value upon Ir SA anchoring which confirm the increase in valence state of the Ni and Fe. The calculated COHP value of Ir_{SA}-NiFe-LDH (−1.074) as compared to NiFe-LDH (−1.048) inferring the increased covalency in TM–O bond (Fig. 6f). This can be attributed to the increased valence state of the TM, which effectively reduces the Δ_χ difference between the metal and oxygen. DOS calculation reveals a notable upward shifting of O 2p band to −2.291 eV in Ir_{SA}-NiFe-LDH from −3.827 eV towards the Fermi level and thereby enhancing the flow electrons from the oxide ligand. This facilitate the release

of lattice oxygen and thereby follows the LOM for OER. In another work Zheng and co-worker activated the lattice oxygen of a high entropy MnFeCoNiCu-LDH *via* surface anchoring of Au SA *via* electrochemical reduction method (Fig. 6g).[77] The Au_{SA}-MnFeCoNiCu-LDH demand a lower overpotential value of 213 mV as compared to pristine LDH which required an overpotential value of 323 mV to drive 10 mA cm^{-2} current density. The improved activity of SA decorated LDH was ascribed to change in reaction mechanism from AEM to LOM and thereby reduces the activation energy barrier. XAS analysis reveals that compared with metals in MnFeCoNiCu-LDH the K-edge absorption spectrum shift to higher energy in Au_{SA}-MnFeCoNiCu-LDH, inferring an increased valence state upon Au SA anchoring. Considering the highest electronegativity of Au (2.54), the positively polarized Au SA drag the electron density from the 3d TM ions and thereby promotes the lattice oxygen through higher covalency. Importance of this electronegativity difference was further rationalize by anchoring different SAs such as Ru, Pt, and Ag with respective electronegativity values of 2.2, 2.3, and 1.9 over MnFeCoNiCu-LDH. Electrochemical results validates that incorporating SAs with higher electronegativity is more conductive to trigger the LOM in the LDH. Theoretical analysis indicates that the strong electron-withdrawing character of Au single atoms intensifies TM–O covalency, causing contraction of the metal d orbitals and a concomitant increase in on-site Coulomb repulsion. This electronic compression downshifts the lower Hubbard band toward the O 2p manifold, enhancing metal–oxygen orbital overlap and rendering lattice oxygen electronically accessible for redox participation (Fig. 6h).

6. Unifying electronic origin of LOM activation: valence-state modulation as the central lever

From the above discussion it is evident that various surface engineering strategies, including cation and anion doping, interlayer anion modulation, heterostructure engineering, and single-atom annexation, all lead to a common electronic effect: controlling the valence state of the active transition-metal center (Fig. 7a–e).[78–81] This adjustment of the valence state lowers the charge-transfer energy (Δ), activates or raises O 2p states, and lowers the lower Hubbard band (LHB) due to increased on-site Coulomb repulsion (U). Even though these methods seem chemically different, they produce similar electronic structures that encourage lattice oxygen participation during the oxygen evolution reaction (OER). However, this convergence doesn't happen by directly tuning oxygen electronic states. In oxides or in LDH structure, the high electronegativity of oxygen and the rigid ligand framework limit the independent adjustment of O-derived bands. This results in the oxygen sublattice mostly reacting passively to changes in metal-centered electronics. Notably three important prerequisites (cited in Section 4.1) are mainly determined by the valence state of the active metal. Increasing the oxidation state stabilizes and lowers the metal d band, enhances orbital contraction and on-site Coulomb repulsion (U), and strengthens TM–O covalency. Together, these effects reduce Δ and enhance the overlap between the LHB and the O 2p manifold, making lattice oxygen redox-active. Thus, while surface and structural engineering offer various experimental approaches, their ability to promote LOM ultimately depends on one main principle: adjusting the metal valence state is the key factor that controls oxygen redox accessibility in LDHs and related oxide/hydroxide catalysts.

7. What distinguishes LOM from an optimized AEM when electronic prerequisites are similar?

In the current scenario with great advancement in the field of catalyst development it is notable that many superior OER catalysts with elevated metal oxidation states and strong TM–O covalency, yet still follow the AEM rather than LOM. This raises a fundamental question: if the occurrence of high valency on TM ions and strong covalency in TM–O bond ensures the lattice oxygen activation, why do they so often result only in faster adsorbate chemistry? The answer lies in whether ligand activation is accommodated or hindered by the structural rigidity of the catalyst during oxygen turnover. In AEM pathway the enhanced covalency stabilizes high-valent metal-oxo intermediates, while oxygen remains electronically passive and structurally conserved. The strong covalency induced electron withdrawal from oxygen is transient and accelerate the O–O coupling with the incoming electrolyte ions. Consequently, AEM does not need lattice oxygen removal, vacancy formation, or lattice reorganization.

In contrast, LOM imposes an additional and far more demanding requirement: lattice oxygen must not only participate in redox but must also physically leave the lattice as O_2, creating a transient oxygen vacancy that must be stabilized and subsequently refilled by electrolyte species. This introduces a structural criterion that is absent in AEM. Thus, LOM activation requires two simultaneous conditions: (1) oxygen ligands must be redox-accessible (high TM valence, strong covalency, favorable band alignment); and (2) structural condition: the lattice must be sufficiently flexible to tolerate oxygen removal, stabilize vacancy formation, and allow rapid refilling from the electrolyte without catastrophic destabilization. LOM is therefore not simply a more covalent or more oxidized version of AEM. It represents a qualitatively different regime in which the lattice itself becomes a dynamic reactant rather than a static scaffold. When structural flexibility is insufficient, even catalysts that meet all electronic prerequisites for oxygen redox will revert to an optimized AEM pathway.[82–89]

In this regard LDHs their soft, layered architecture, weakly ionic M–OH bonding, intrinsic hydration, and dynamic hydrogen-bonded interlayer environment collectively enable local lattice relaxation upon oxygen removal. The structural permissiveness of LDHs towards lattice oxygen removal is directly supported by our previous theoretical analysis on Ru cluster decorated NiV-LDH.[90] Although the oxygen vacancy kinetics was thermodynamically endothermic, the energetic

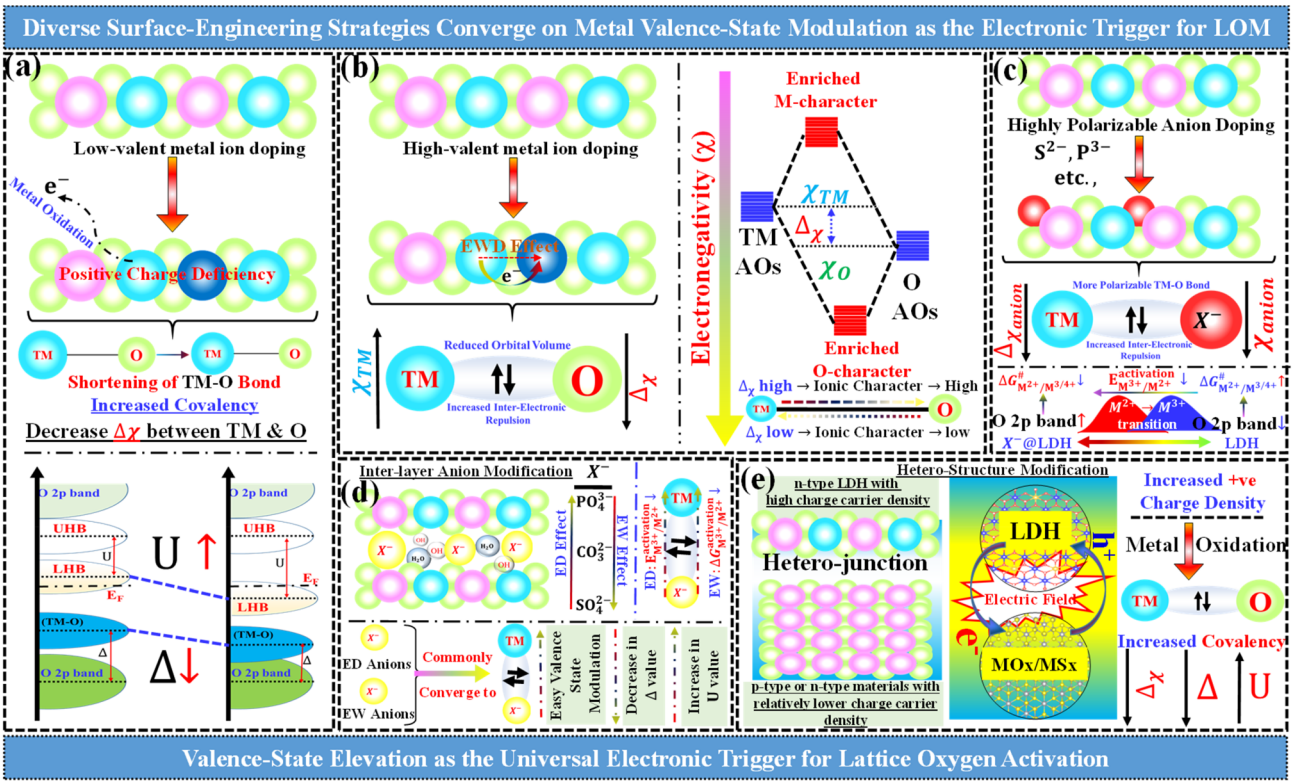

Fig. 7 Various surface engineering strategies for enforcing lattice oxygen activation in LDH-based electrocatalysts. (a) Adding low-valent metal ions increases TM–O covalency and directly triggers lattice oxygen activation; (b) *in situ* electrochemical oxidation of active metal centers changes the covalency in high-valent metal-doped LDHs, driving lattice oxygen redox; (c) doping with highly polarizable anions reduces the potential needed for metal activation and promotes lattice oxygen participation; (d) intercalating electron-donating and electron-withdrawing anions systematically adjusts the metal valence and electronic structure, controlling lattice oxygen activation; and (e) heterostructural surface engineering changes the local coordination and electronic environment to activate lattice oxygen. Together, these surface modification strategies are not mechanistically distinct but electronically similar. They all promote lattice oxygen activation by altering the valence state of the active metal and strengthening TM–O covalency. This establishes a unified electronic requirement for lattice oxygen-involved catalysis in LDH systems.

penalty is substantially reduced in the presence of Ru-based cluster. Which indicating that nanoscale hetero-structuring lowers the lattices strain associated with oxygen removal. Moreover, the oxygen deficient LDH structures were energetically stabilized more with hetero-structure entity. This suggesting the ability of LDH lattice to locally relax and redistribute charge following oxygen removal.

Moreover, interlayer anions and water molecules can electrostatically and chemically stabilize emerging oxygen vacancies and facilitate their rapid refilling by OH^- or H_2O from the electrolyte. For example, Ren *et al.* demonstrated that oxygen vacancy formation in NiFe-LDH is strongly governed by the nature of the interlayer anions.[91] By introducing SO_4^{2-} ions, they achieved an optimal concentration of oxygen vacancies through a low-energy formation pathway, highlighting the critical role of interlayer chemistry in regulating oxygen dynamics. This illustrates that LDHs provide a uniquely tunable structural and chemical platform in which interlayer species can be deliberately engineered to control vacancy formation, stabilization, and healing-a prerequisite for sustaining the cyclic oxygen exchange intrinsic to the LOM. In essence, LOM emerges only when electronic activation of oxygen is matched by structural tolerance to oxygen exchange (Fig. 8). Here the structural tolerance is defined as the ability of a material framework to accommodate reversibly oxygen vacancy formation and TM–O bond arrangement under oxidizing conditions without suffering from catastrophic material degradation (Fig. 9). Experimentally, flexibility may be quantified by reversible lattice distortion under *operando* XRD/XAS characterization and Raman softening of TM–O bonds, as well as dynamic oxygen exchange rates. Computational descriptors of flexibility include oxygen vacancy formation energies with moderate magnitude, increased TM–O bond covalency, and softening of phonon modes and stability under *ab initio* simulations of oxidative conditions.

8. Future outlook and conclusions

The chemistry framework discussed here changes the focus of lattice oxygen activation from simply being an observation to becoming a vital design principle. By identifying transition-metal valence regulation as a crucial electronic factor and lattice flexibility as the necessary structural support, we can deliberately design LDH-based catalysts for controlled LOM

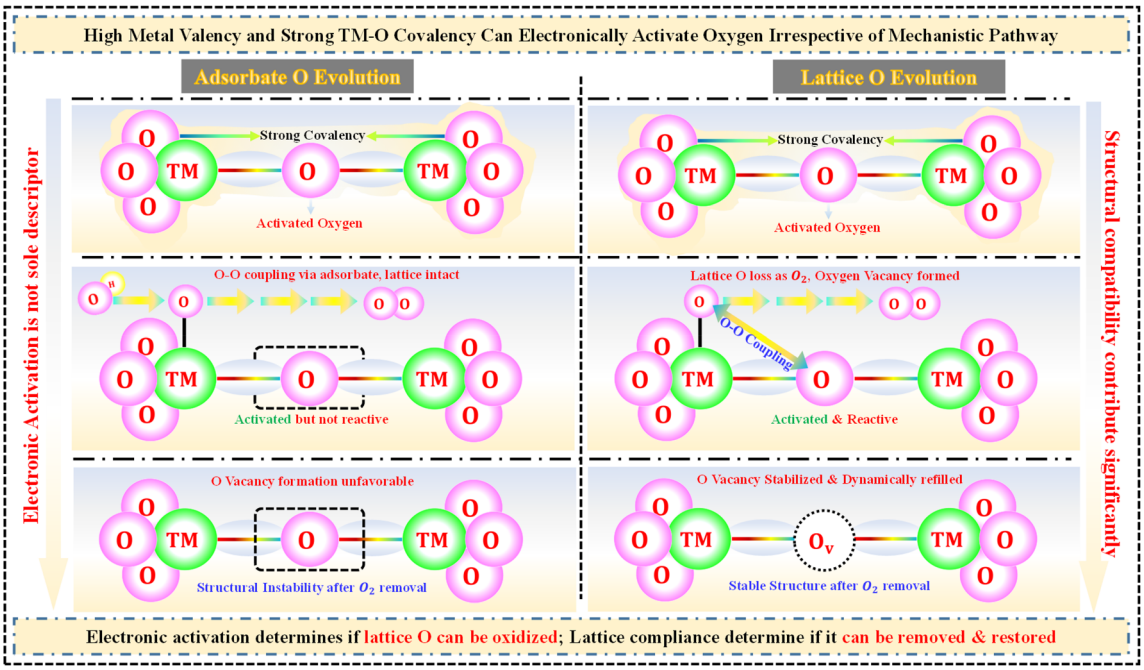

Fig. 8 Schematic comparison of an optimized adsorbate evolution mechanism (AEM) and a lattice oxygen mechanism (LOM) under similar electronic activation. In both systems, high metal valence and strong TM–O covalency activate lattice oxygen. In optimized AEM catalysts, O–O bond formation happens through surface adsorbates while the lattice stays intact and creating oxygen vacancies is unfavorable. In contrast, LOM includes direct participation and release of lattice oxygen as O_2, creating temporary oxygen vacancies that are stabilized and quickly repaired in structurally compliant lattices like layered double hydroxides.

operation. This replaces traditional trial-and-error approaches. It opens up several specific and chemically diverse pathways for future catalyst development, including:

(1) An unexplored opportunity in LDHs is the substitution of low-valent cations, like Li^+, Mg^{2+}, and Al^{3+}, in the redox-active Ni/Co/Fe layers. This approach helps achieve internal charge compensation by oxidizing active metals. While this method works well in oxides, it has not been thoroughly explored in LDH chemistry. Low valent ion doping offers a straightforward way to activate the metal ions to higher oxidation states without needing increased external potential, making LOM achievable under milder electrochemical conditions. Careful analysis of the dopant identity, concentration, and spatial distribution may create a reliable connection between dopant chemistry, metal valence, Δ reduction, and LOM initiation.

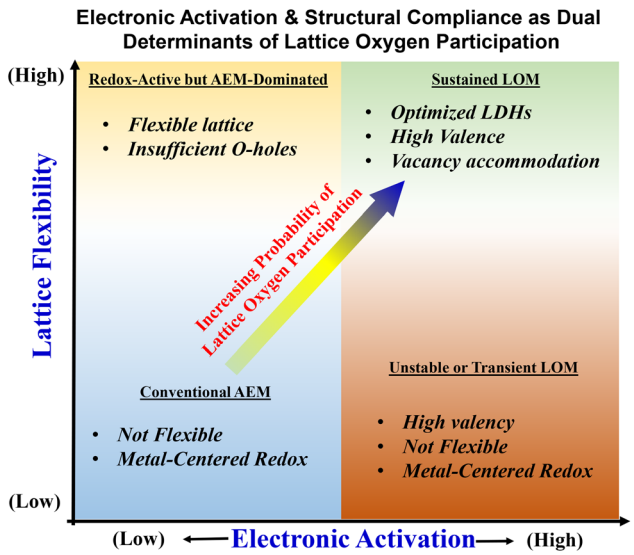

Fig. 9 Conceptual map showing the role of lattice oxygen participation as controlled by two parameters: electronic activation (TM valence and TM–O covalency), and structural compliance (accommodation of reversible vacancies), and placing AEM and LOM as end-member cases within a mechanistic spectrum.

(2) LDHs provide a unique chance for chemical adjustments through anion substitution and intercalation, which allows for indirect control of oxygen electronics. Electron-withdrawing anions, such as F^- and SO_4^{2-}, can stabilize high-valent metal centers and lower Δ. In contrast, polarizable anions like S^{2-}, P^{3-}, and Se^{2-} can enhance ligand p-states and improve access to oxygen redox. Anions between layers also help influence vacancy stabilization and repair kinetics, which are crucial for maintaining LOM. Future research should treat anions as active electronic and structural regulators of lattice oxygen chemistry.

(3) Creating heterostructures enables the spatial separation and pairing of electronic functions. By combining LDHs with p-type or low-donor-density n-type materials the direction and amount of charge transfer can be alter. This facilitates selective oxidation of lattice oxygen rather than the metal center. Electronic conflicts at the interface might effectively encourage systems to shift from the AEM to the LOM state.

(4) Nano-structuring and adding single atoms provide localized ways to disrupt standard metal-centered redox processes. This creates electronic disparities and strong local

covalency. Such methods could serve as precise triggers for oxygen hole formation while keeping the overall lattice intact, which is essential for long-term stability.

(5) Though LOM can lower kinetic barriers, it introduces new stability challenges regarding oxygen vacancy formation, lattice distortion, and potential irreversible oxygen loss. LDHs have an advantage here; their soft lattice, hydration properties, and dynamic interlayer setup support reversible vacancy formation, stabilization, and healing. Future catalyst designs should specifically consider: (a) reversible vacancy formation energies; (b) quick vacancy healing from electrolyte OH^-/H_2O; and (c) prevention of irreversible metal dissolution or phase changes.

(6) Since LDHs already perform effectively in alkaline and AEM electrolyzers, applying LOM chemistry to LDH platforms offers a practical path for industrial use. Smart activation of lattice oxygen could lower overpotentials, reduce the energy required per kilogram of H_2, and improve efficiency without relying on rare noble metals.

(7) It is worth mentioning that AEM and LOM should not be thought of as completely distinct mechanisms but rather as two extremes in a continuum in which the degree of lattice oxygen participation can coexist under the same electrochemical conditions. Therefore, the overlap in these mechanisms should be understood to arrive at a more realistic understanding of the catalysis process.

In summary, this Perspective redefines LOM from a rare or complicated process to a chemically achievable state that can be intentionally engineered through valence-state control and lattice design. LDHs present a flexible platform that allows simultaneous tuning of electronic activation and structural adaptation. This dual approach can deepen our understanding of oxygen redox chemistry and provide practical strategies to enhance scalable and efficient hydrogen production.

Author contributions

Arun Karmakar: conceptualization, writing – original draft, review & editing. Asha K. Satheesan: review & editing. Subrata Kundu: funding acquisition, supervision, writing – review & editing.

Conflicts of interest

There are no conflicts to declare.

Data availability

No primary research results, software or code have been included and no new data were generated or analysed as part of this review.

Acknowledgements

Asha K. Satheesan Wishes to acknowledge University Grant Commision (UGC) for Junior Research Fellowship (JRF). Subrata Kundu wish to acknowledge the DST for CRG (Core Research Grant) funding of number # CRG/2021/001089 dated November 20th, 2021. CSIR-CECRI manuscript number: CECRI/PESVC/Pubs./2026-018.

References

1 J. Song, C. Wei, Z. F. Huang, C. Liu, L. Zeng, X. Wang and Z. J. Xu, *Chem. Soc. Rev.*, 2020, **49**, 2196.
2 J. H. Montoya, L. C. Seitz, P. Chakthranont, A. Vojvodic, T. F. Jaramillo and J. K. Nørskov, *Nat. Mater.*, 2016, **16**, 70–81.
3 S. Anantharaj, S. R. Ede, K. Sakthikumar, K. Karthick, S. Mishra and S. Kundu, *ACS Catal.*, 2016, **6**, 8069–8097.
4 S. Anantharaj, S. R. Ede, K. Karthick, S. Sam Sankar, K. Sangeetha, P. E. Karthik and S. Kundu, *Energy Environ. Sci.*, 2018, **11**, 744–771.
5 M. T. M. Koper, *Chem. Sci.*, 2013, **4**, 2710–2723.
6 B. Zhang, X. Zheng, O. Voznyy, R. Comin, M. Bajdich, M. García-Melchor, L. Han, J. Xu, M. Liu, L. Zheng, F. Pelayo García De Arquer, C. T. Dinh, F. Fan, M. Yuan, E. Yassitepe, N. Chen, T. Regier, P. Liu, Y. Li, P. De Luna, A. Janmohamed, H. L. Xin, H. Yang, A. Vojvodic and E. H. Sargent, *Homogeneously dispersed multimetal oxygen-evolving catalysts*, 2016, vol. 352, p. 6283.
7 N. Zhang and Y. Chai, *Energy Environ. Sci.*, 2021, **14**, 4647–4671.
8 K. S. Exner, *ChemCatChem*, 2021, **13**, 4066–4074.
9 X. Ren, Y. Zhai, N. Yang, B. Wang and S. Liu, *Adv. Funct. Mater.*, 2024, **34**, 2401610.
10 A. Grimaud, W. T. Hong, Y. Shao-Horn and J. M. Tarascon, *Nat. Mater.*, 2016, **15**, 121–126.
11 C. Rong, X. Huang, H. Arandiyan, Z. Shao, Y. Wang and Y. Chen, *Adv. Mater.*, 2025, **37**, 2416362.
12 N. Zhang and Y. Xiong, *J. Phys. Chem. C*, 2023, **127**, 2147–2159.
13 J. Jiang, F. Sun, S. Zhou, W. Hu, H. Zhang, J. Dong, Z. Jiang, J. Zhao, J. Li, W. Yan and M. Wang, *Nat. Commun.*, 2018, **9**, 2885.
14 C. Rong, X. Huang, H. Arandiyan, Z. Shao, Y. Wang and Y. Chen, *Adv. Mater.*, 2025, **37**, 2416362.
15 H. Adamu, S. I. Abba, P. B. Anyin, Y. Sani, Z. H. Yamani and M. Qamar, *ACS Mater. Lett.*, 2023, **5**, 299–320.
16 Y. Zuo, D. Rao, S. Ma, T. Li, Y. H. Tsang, S. Kment and Y. Chai, *ACS Nano*, 2019, **13**, 11469–11476.
17 S. Iqbal, J. C. Ehlers, I. Hussain, K. Zhang and C. Chatzichristodoulou, *Chem.–Eng. J.*, 2024, **499**, 156219.
18 L. Lv, Z. Yang, K. Chen, C. Wang and Y. Xiong, *Adv. Energy Mater.*, 2019, **9**, 1803358.
19 A. Karmakar, K. Karthick, S. S. Sankar, S. Kumaravel, R. Madhu and S. Kundu, *J. Mater. Chem. A*, 2021, **9**, 1314–1352.
20 Y. Wang, C. Chen, X. Xiong, S. A. Skaanvik, Y. Zhang, E. D. Bøjesen, Z. Wang, W. Liu and M. Dong, *J. Am. Chem. Soc.*, 2024, **146**, 17032–17040.
21 D. K. Cho, H. W. Lim, A. Haryanto, B. Yan, C. W. Lee and J. Y. Kim, *ACS Nano*, 2024, **18**, 20459–20467.
22 D. Zhou, P. Li, X. Lin, A. McKinley, Y. Kuang, W. Liu, W. F. Lin, X. Sun and X. Duan, *Chem. Soc. Rev.*, 2021, **50**, 8790.

23 Y. Luo, Z. Zhang, M. Chhowalla and B. Liu, *Adv. Mater.*, 2022, **34**, 2108133.
24 R. Chen, S. F. Hung, D. Zhou, J. Gao, C. Yang, H. Tao, H. Bin Yang, L. Zhang, L. Zhang, Q. Xiong, H. M. Chen and B. Liu, *Adv. Mater.*, 2019, **31**, 1903909.
25 Y. Wang, M. Zhang, Y. Liu, Z. Zheng, B. Liu, M. Chen, G. Guan and K. Yan, *Adv. Sci.*, 2023, **10**, 2207519.
26 R. Zhao, S. Xu, D. Liu, L. Wei, S. Yang, X. Yan, Y. Chen, Z. Zhou, J. Su, L. Guo and C. Burda, *Appl. Catal., B*, 2023, **338**, 123027.
27 Y. Bi, Z. Cai, D. Zhou, Y. Tian, Q. Zhang, Q. Zhang, Y. Kuang, Y. Li, X. Sun and X. Duan, *J. Catal.*, 2018, **358**, 100–107.
28 Z. Cai, D. Zhou, M. Wang, S. M. Bak, Y. Wu, Z. Wu, Y. Tian, X. Xiong, Y. Li, W. Liu, S. Siahrostami, Y. Kuang, X. Q. Yang, H. Duan, Z. Feng, H. Wang and X. Sun, *Angew. Chem., Int. Ed.*, 2018, **57**, 9392–9396.
29 X. Tang, Y. Li, X. Jiang, H. Li, Y. Wang and X. Wang, *J. Electroanal. Chem.*, 2025, **982**, 118996.
30 D. Zhou, Z. Cai, Y. Jia, X. Xiong, Q. Xie, S. Wang, Y. Zhang, W. Liu, H. Duan and X. Sun, *Nanoscale Horiz.*, 2018, **3**, 532–537.
31 B. M. Hunter, W. Hieringer, J. R. Winkler, H. B. Gray and A. M. Müller, *Energy Environ. Sci.*, 2016, **9**, 1734–1743.
32 J. R. Huang, M. Y. Xie, M. H. Xian, Y. Luo, J. H. Nie, Z. Y. Ou-Yang, Q. X. Wang, G. F. Huang and W. Q. Huang, *Appl. Phys. Lett.*, 2025, **127**, 103905.
33 Z. Li, G. Lin, L. Wang, H. Lee, J. Du, T. Tang, G. Ding, R. Ren, W. Li, X. Cao, S. Ding, W. Ye, W. Yang and L. Sun, *Nat. Catal.*, 2024, **7**, 944–952.
34 A. Seijas-Da Silva, A. Hartert, V. Oestreicher, J. Romero, C. Jaramillo-Hernández, L. J. J. Muris, G. Thorez, B. J. C. Vieira, G. Ducourthial, A. Fiocco, S. Legendre, C. Huck-Iriart, M. Mizrahi, D. López-Alcalá, A. T. S. Freiberg, K. J. J. Mayrhofer, J. C. Waerenborgh, J. J. Baldoví, S. Cherevko, M. Varela, S. Thiele, V. Lloret and G. Abellán, *Nat. Commun.*, 2025, **16**, 6138.
35 H. J. Niu, N. Ran, W. Zhou, W. An, C. Huang, W. Chen, M. Zhou, W. F. Lin, J. Liu and L. Guo, *J. Am. Chem. Soc.*, 2025, **147**, 2607–2615.
36 X. He, Y. Yao, L. Zhang, H. Wang, H. Tang, W. Jiang, Y. Ren, J. Nan, Y. Luo, T. Wu, F. Luo, B. Tang and X. Sun, *Nat. Commun.*, 2025, **16**, 4998.
37 X. Sun, W. Shen, H. Liu, P. Xi, M. Jaroniec, Y. Zheng and S. Z. Qiao, *Nat. Commun.*, 2024, **15**, 10351.
38 J. Zhang, X. Zhang, Z. Ma, K. Fang, L. Wang, H. Ni and B. Zhao, *ACS Catal.*, 2025, **15**, 6486–6496.
39 Z. Cai, J. Liang, Z. Li, T. Yan, C. Yang, S. Sun, M. Yue, X. Liu, T. Xie, Y. Wang, T. Li, Y. Luo, D. Zheng, Q. Liu, J. Zhao, X. Sun and B. Tang, *Nat. Commun.*, 2024, **15**, 6624.
40 P. Zhai, C. Wang, Y. Zhao, Y. Zhang, J. Gao, L. Sun and J. Hou, *Nat. Commun.*, 2023, **14**, 1873.
41 X. Kang, F. Yang, Z. Zhang, H. Liu, S. Ge, S. Hu, S. Li, Y. Luo, Q. Yu, Z. Liu, Q. Wang, W. Ren, C. Sun, H. M. Cheng and B. Liu, *Nat. Commun.*, 2023, **14**, 3607.
42 Y. Zhu, J. Wang, G. Weiser, M. Klingenhof, T. Koketsu, S. Liu, Y. Pi, G. Henkelman, X. Shi, J. Li, C. W. Pao, M. H. Yeh, W. H. Huang, P. Strasser and J. Ma, *Adv. Energy Mater.*, 2025, **15**, 2500554.
43 T. Jiang, X. Jiang, C. Jiang, J. Wang, Y. Danlos, T. Liu, C. Deng, C. Chen, H. Liao and V. Kyriakou, *Adv. Energy Mater.*, 2025, **15**, 2501634.
44 S. Pal, E. Chaturvedi, C. Das, N. Sinha, T. Ahmed and P. Roy, *Nanoscale*, 2025, **17**, 12094–12107.
45 Y. Zhao, Q. Wen, D. Huang, C. Jiao, Y. Liu, Y. Liu, J. Fang, M. Sun and L. Yu, *Adv. Energy Mater.*, 2023, **13**, 2203595.
46 W. Li, Y. Ding, Y. Zhao, Z. Li, G. Lin, L. Wang and L. Sun, *Angew. Chem.*, 2025, **137**, e202505924.
47 Y. Shi, L. Song, Y. Liu, T. Wang, C. Li, J. Lai and L. Wang, *Adv. Energy Mater.*, 2024, **14**, 2402046.
48 F. Wu, F. Tian, M. Li, S. Geng, L. Qiu, L. He, L. Li, Z. Chen, Y. Yu, W. Yang and Y. Hou, *Angew. Chem., Int. Ed.*, 2025, **64**, e202413250.
49 J. Zhao, N. Liao and J. Luo, *J. Mater. Chem. A*, 2023, **11**, 9682–9690.
50 Y. Xu, K. Xu, H. Tan, H. Huang, F. Lin, C. Zhang, J. Wang, R. Ran, J. Zeng, Z. Yu, S. M. Thalluri, L. Meng, D. Xiong and L. Liu, *J. Mater. Chem. A*, 2025, **13**, 14822–14835.
51 Z. Y. Liu, J. J. Ge, L. Yu, S. H. Ong, L. J. Zhang and J. M. Hu, *Small*, 2025, **21**, 2504076.
52 J. Song, C. Wei, Z. F. Huang, C. Liu, L. Zeng, X. Wang and Z. J. Xu, *Chem. Soc. Rev.*, 2020, **49**, 2196.
53 W. Xu, M. Andersen and K. Reuter, *ACS Catal.*, 2021, **11**, 734–742.
54 Y. Surendranath, M. W. Kanan and D. G. Nocera, *J. Am. Chem. Soc.*, 2010, **132**, 16501–165099.
55 A. Grimaud, O. Diaz-Morales, B. Han, W. T. Hong, Y. L. Lee, L. Giordano, K. A. Stoerzinger, M. T. M. Koper and Y. Shao-Horn, *Nat. Chem.*, 2017, **9**, 457–465.
56 D. B. Hibbert and C. R. Churchill, *Kinetics of the Electrochemical Evolution of Isotopically Enriched Gases in Alkaline Solution*, 1984, vol. 80.
57 S. Fierro, T. Nagel, H. Baltruschat and C. Comninellis, *Electrochem. commun.*, 2007, **9**, 1969–1974.
58 K. Macounova, M. Makarova and P. Krtil, *Electrochem. commun.*, 2009, **11**, 1865–1868.
59 M. Y. Xie, J. R. Huang, H. Wan, J. Nie, M. H. Xian, Z. Y. Ou-Yang, G. F. Huang and W. Q. Huang, *Appl. Phys. Lett.*, 2025, **126**, 153901.
60 N. Zhang and Y. Chai, *Energy Environ. Sci.*, 2021, **14**, 4647–4671.
61 Y. Fan, R. Li, Y. Wu, Y. Li, H. Xu, P. Ren, F. Meng, J. Zhang, M. An and P. Yang, *J. Alloys Compd.*, 2024, **1008**, 176678.
62 Z. He, J. Zhang, Z. Gong, H. Lei, D. Zhou, N. Zhang, W. Mai, S. Zhao and Y. Chen, *Nat. Commun.*, 2022, **13**, 2191.
63 J. Wang, Z. Xing, R. Kang, Y. Zheng, Z. Zhang, T. Ma, Y. Wang, B. Yin, Y. Liao, L. Li, C. Cheng and S. Li, *Adv. Funct. Mater.*, 2025, **35**, 2418439.
64 Y. Zhou, J. Zeng, X. Zheng, W. Huang, Y. Dong, J. Zhang, Y. Deng and R. Wu, *J. Colloid Interface Sci.*, 2025, **678**, 536–546.
65 J. T. Mefford, X. Rong, A. M. Abakumov, W. G. Hardin, S. Dai, A. M. Kolpak, K. P. Johnston and K. J. Stevenson, *Nat. Commun.*, 2016, **7**, 11053.

66 S. Song, Y. Wang, P. Tian and J. Zang, *J. Colloid Interface Sci.*, 2025, **677**, 853–862.
67 Q. Su, P. Wang, Q. Liu, R. Sheng, W. Cheng, J. Ding, Y. Lei and Y. Huang, *Appl. Catal., B*, 2024, **351**, 123994.
68 W. Xu, M. Andersen and K. Reuter, *ACS Catal.*, 2021, **11**, 734–742.
69 Q. Yang, Y. Li, A. Kong, Y. Li, T. An, C. Yang, Y. Zhao, L. Lai, C. Feng, X. Zhou, P. Chen, K. Pan, Z. Wang, H. Huang and F. Yu, *Appl. Catal., B*, 2025, **383**, 126130.
70 Y. Li, J. Liu, S. Li and S. Peng, *ACS Catal.*, 2024, **14**, 4807–4819.
71 H. Xiao, H. Shin and W. A. Goddard, *Proc. Natl. Acad. Sci. U. S. A.*, 2018, **115**, 5872–5877.
72 J. Zhang, Y. Jin, Z. Xu, Y. Du, Y. Xu, X. Ren, B. Xue, D. Liu, Y. Zhu and F. Li, *ACS Sustain. Chem. Eng.*, 2025, **13**, 15177–15188.
73 Y. Cao, Q. Wang, Z. Wang, J. Gao, G. Lv, N. Du, Y. Liu, X. Wang and F. Cao, *Chem. Eng. J.*, 2025, **516**, 163929.
74 K. Wang, H. Xu, B. Huang, H. Xing, L. Jin, X. Qian, H. Chen and G. He, *Small*, 2025, **21**, 2411790.
75 J. Huang, R. Gao, B. Wang, X. Cui, L. Pan, Z. F. Huang, X. Zhang and J. J. Zou, *Chem. Eng. Sci.*, 2025, **311**, 121606.
76 Z. Duan, Z. Cui, Z. Gao, W. Xu, Y. Liang, H. Jiang, Z. Li, F. Wang and S. Zhu, *ACS Catal.*, 2025, **15**, 16882–16892.
77 F. Wang, P. Zou, Y. Zhang, W. Pan, Y. Li, L. Liang, C. Chen, H. Liu and S. Zheng, *Nat. Commun.*, 2023, **14**, 6019.
78 R. Mehmood, W. Fan, X. Hu, J. Li, P. Liu, Y. Zhang, Z. Zhou, J. Wang, M. Liu and F. Zhang, *J. Am. Chem. Soc.*, 2023, **145**, 12206–12213.
79 R. Liang, B. Zhang, Y. Du, X. Han, S. Li and P. Xu, *ACS Catal.*, 2023, **13**, 8821–8829.
80 H. Wang, T. Zhai, Y. Wu, T. Zhou, B. Zhou, C. Shang and Z. Guo, *Adv. Sci.*, 2023, **10**, 2301706.
81 Y. Ou, L. P. Twight, B. Samanta, L. Liu, S. Biswas, J. L. Fehrs, N. A. Sagui, J. Villalobos, J. Morales-Santelices, D. Antipin, M. Risch, M. C. Toroker and S. W. Boettcher, *Nat. Commun.*, 2023, **14**, 7688.
82 T. Zhang, H. F. Zhao, Z. J. Chen, Q. Yang, N. Gao, L. Li, N. Luo, J. Zheng, S. Da Bao, J. Peng, X. Peng, X. W. Liu and H. Bin Yu, *Nat. Commun.*, 2025, **16**, 3327.
83 Y. H. Wang, L. Li, J. Shi, M. Y. Xie, J. Nie, G. F. Huang, B. Li, W. Hu, A. Pan and W. Q. Huang, *Adv. Sci.*, 2023, **10**, 2303321.
84 S. Wu, W. Lu, S. Zhao, K. Zhao, N. Yan, L. Huang, D. Li, T. Jiang, H. Wu and F. Ren, *Adv. Sci.*, 2025, e15407.
85 N. Zhang, X. Feng, D. Rao, X. Deng, L. Cai, B. Qiu, R. Long, Y. Xiong, Y. Lu and Y. Chai, *Nat. Commun.*, 2020, **11**, 4066.
86 Y. Zhu, Y. Zhao, C. Xi, K. Hu, S. Han and J. Jiang, *Composites, Part B*, 2025, **298**, 112356.
87 Y. Zhai, X. Ren, Y. Sun, D. Li, B. Wang and S. Frank) Liu, *Appl. Catal., B*, 2023, **323**, 122091.
88 Y. Xu, Y. Li, Y. Du, J. Zhang, S. Li, C. Zhang, X. Ren, Z. Xu, B. Xue and F. Li, *Chem.–Eng. J.*, 2025, **522**, 168037.
89 D. Shi, Y. Ji, F. Lu, J. Yao, S. Zhang and P. Zhang, *Inorg. Chem. Front.*, 2023, **10**, 5391–5405.
90 A. Karmakar, K. Karthick, S. S. Sankar, S. Kumaravel, R. Madhu, K. Bera, H. N. Dhandapani, S. Nagappan, P. Murugan and S. Kundu, *J. Mater. Chem. A*, 2022, **10**, 3618–3632.
91 L. Ren, Y. Wei, S. Yu, R. Li, L. Chen and T. Qiang, *ACS Appl. Nano Mater.*, 2025, **8**, 3152–3162.